RSC Advances

ROYAL SOCIETY
OF CHEMISTRY

www.rsc.org/advances

Development of a novel magnetite-chitosan composite for the removal of fluoride from drinking water: Adsorption modeling and optimization

Anoushiravan Mohseni-Bandpi[1], Babak Kakavandi[2], Roshanak Rezaei Kalantary[3, *], Ali Azari[4], Azam Keramati[4]

[1]Department of Environmental Health Engineering, School of Public Health, Shahid Beheshti University of Medical Sciences, Tehran, Iran
[2]Department of Environmental Health Engineering, School of Health, Ahvaz Jundishapur University of Medical Sciences, Ahvaz, Iran
[3]Department of Environmental Health Engineering, School of Public Health, Iran University of Medical Sciences, Tehran, Iran
[4]Department of Environmental Health Engineering, School of Public Health, Tehran University of Medical Sciences, Tehran, Iran

* Corresponding author: Department of Environmental Health Engineering, School of Public Health, Iran University of Medical Sciences, Tehran, Iran
Email: r-rezaei@tums.ac.ir
Tel: +98 21 86704633, Fax: +98 21 86709487

Abstract

Magnetic nanoparticles (MNPs) have recently been adopted by researchers in the field of adsorption/biosorption for separation of pollutants from aqueous solutions. In this paper, chitosan was impregnated with magnetite nanoparticles through a chemical co-precipitation method to fabricate hybrid adsorbents of Fe_3O_4-chitosan. The physicochemical and structural properties of the adsorbent were characterized, and then the performance of the adsorbent was evaluated for fluoride removal from water. The operational factors affecting the adsorption process, including pH, contact time, adsorbent dosage, initial fluoride concentration, and temperature, were studied. Various isotherm and kinetic models were also used to evaluate the fitness of the experimental data with the modeled results. The

1

equilibrium data were well described by the Freundlich model. The kinetic of the adsorption process followed the pseudo-second-order model. Recycling results suggested that the Fe_3O_4-chitosan particles maintain a great reusability potential for five consecutive cycles. Findings also showed that the Fe_3O_4-chitosan can be easily regenerated via acid treatment. The results of the present work highlighted the potential of using Fe_3O_4-chitosan magnetic composite for the removal of fluoride from water. In conclusion, Fe_3O_4-chitosan can be considered as an appropriate adsorbent for fluoride removal from water, because it can be separated both quickly and easily, it has high efficiency, and that it does not lead to secondary pollution.

Keywords: Magnetite nanoparticles, Chitosan, Adsorption, Magnetic separation, Fluoride

1. Introduction

Fluoride existing in drinking water can be either detrimental or beneficial to human health, depending solely on its concentration in water [1]. The beneficial effects of fluoride, primarily on health and bones, are observed at lower concentration; at higher concentrations, however, fluoride can cause fluorosis, which can affect organ, tissue, or cell in the body; however, the primary health impacts associated with excessive intake of fluoride are dental and skeletal fluorosis [2]. The World Health Organization (WHO) has, therefore, set a guideline value for the safe level of fluoride in drinking water, 1.5 mg/L [1]. Hence, it is quite critical to remove the excessive amounts of fluoride from drinking water.

A wide variety of methods have been used to remove fluoride from drinking water, including adsorption and biosorption [3, 4], chemical precipitation mostly with calcium and aluminum salts [5, 6], ion exchange, and membrane process such as reverse osmosis, nanofiltration, and electrodialysis [7, 8]. All these methods have proven efficient; however, adsorption is the most

widely used method for the removal of excessive fluoride from water, due primarily to its low costs, high efficiency, and being environmentally friendly [9].

During the past few years, a large number of studies have been carried out on the efficiency of composite materials that contain natural polymers and have inorganic origins, which have proven effective [9]. Chitosan is a copolymer with favorable biological characteristics, which is also harmless to humans [10]. Due to its excellent adsorption properties, chitosan has been widely used, alone or in combination with other materials, for the removal of a variety of environmental pollutants, including fluoride in drinking water [11, 12]. Other beneficial characteristics of chitosan include its biodegradability, flexibility, hydrophilicity, biocompatibility, and versatility [9]. However, pure chitosan does not have optimal adsorption because it easily dissolves in acidic solution and has weak chemical resistance[13].

Magnetic nanoparticles (MNPs) have recently been adopted by researchers in the field of adsorption/biosorption for separation of pollutants from water [14, 15], mainly because the application of such materials makes the separation of both the adsorbent and the adsorbate much easier from water. Therefore, the water does not need to be filtered or centrifuged after the adsorption process, which is considered a critical advantage. In addition, the sorbent can be easily recovered and reused. Combination of the Fe_3O_4 MNPs and chitosan can effectively avoid the chemical weakness of chitosan. Moreover, the hydroxyl groups on the surface of Fe_3O_4 can interact with amine groups and hydroxyl groups of chitosan through hydrogen-bond interaction to keep chitosan stable under acidic conditions[13] . It is noteworthy that the magnetic chitosan composite has been widely and successfully utilized to remove contaminants such as dye [13, 16], heavy metals[17, 18] , humic acid [19] and uranyl [20].

To the best of our knowledge, few studies have so far been conducted to evaluate the efficiency of magnetic chitosan for fluoride removal from aqueous solutions. Therefore, we aimed at synthesizing a novel magnetic chitosan composite (Fe_3O_4-chitosan) and evaluating

its efficiency for the removal of fluoride from water, which is a major concern in southern parts of Iran.

2. Materials and Methods

2.1. Reagents and equipment

All chemicals were of analytical-laboratory grade, purchased from Merck, and used without further purification. Deionized water (DI-water) was used throughout all the experiments. The pH of the solutions were adjusted by adding 0.1 M hydrochloric acid (HCl) and NaOH. The adsorbent was separated from the solution by using a magnet (dimension, $5 \times 4 \times 4$ cm; intensity, 1.3 T). A UV-Visible spectrophotometer (model CECIL-7100) was used to determine the residual fluoride concentrations in the solution.

2.2. Chitosan extraction

In this work, chitosan was obtained from Shrimp shell wastes, which is available in abundance in southern parts of Iran. Herein, no specific permissions were required for these locations/activities. We also confirm that the field studies did not involve endangered or protected species. First, Shrimp shell was washed with water and put into a 0.5% NaOH solution for 4 h; the shell was then washed with water. It was then dried in an oven at 60 ºC for 2 h and, subsequently, milled and put into a 1 N NaOH solution at 90 ºC for 2 h. In this stage, the weight ratio of powered shrimp shell to solution was 1:20. Afterwards, the remaining shell was washed with deionized water until reaching a neutral pH. In order to separate the inorganic matter from the shell, the remaining shell from the previous stage was put into a 1.4 N HCl solution and kept for 1 h. In this stage, the weight ratio of shell to acid was 1:10. Then, the remaining shell was washed with deionized water until reaching a neutral pH. The extracted chitin was yellow, which was decolorized through acetone washing .

Chitosan was extracted from the chitin using the deacetylation method. For this purpose, the collected chitin was put into a 50% NaOH solution and kept at 100 ºC for 6 h. It was then filtered and washed with deionized water until reaching a neutral pH. The extracted substance, chitosan, was dried at 60 ºC for 1 h. The extracted chitosan , was hydrated and put into a 0.1 M NaOH solution to increase its pH to 8; 0.5 M chloroacetic acid was then added to this solution and the mixture was kept at room temperature for 10 h to change the hydroxyl groups into carboxyl ones. The carboxylated chitosan was then washed with deionized water to reach a neutral pH (Figure 1).

2.3. Synthesis of the Fe_3O_4-chitosan

Magnetic chitosan (Fe_3O_4-chitosan) was prepared using the co-precipitation technique suggested by Du et al. [13] with small modifications. In order to prepare the magnetic chitosan, first DI-water was purged with nitrogen gas in order to provide satisfactory agitation and also prevent the oxidation of ferrous ions for 30 min. Then, dissolved 2.17 g of $FeCl_3.6H_2O$ and 0.77 g of $FeSO_4.7H_2O$ into 50 ml of DI-water under nitrogen atmosphere with vigorous magnetic stirring at 60 ºC for 30 min. Then 0.35 g of chitosan was dissolved in 100 ml of 1% (v/v) acetic acid and added to the above solution. After 120 min of mixing, 48 ml of $NH_3.H_2O$ was added to the mixture drop wisely over 2.0 h until the pH came close to 9. The solution was then vigorously stirred at 100 ºC for 1 h. At the end of reaction, the powder was washed five times with 50 ml DI-water using a magnet. The powder was then air-dried and calcinated at 105±2 ºC for 12 h. We milled and sieved the obtained particles using 0.15 mm standard griddles. Finally, we selected the magnetic chitosan particles using a 1.3 T magnetic field.

2.4. Magnetic chitosan characteristics

The surface morphology of Fe_3O_4-chitosan was analyzed using SEM (MIRA3, Tescan, Czech Republic), at 15 keV. The sample was set in epoxy and placed in the sample chamber and evacuated by high vacuum (5×10^{-7} Torr). The sample was bombarded with a finely focused electron beam. A three dimensional topographic image (SEM micrograph) was formed by collecting the secondary electrons generated by the primary beam [21]. The adsorbent elemental composition was determined using Energy dispersive X-ray (EDX, TESCA MIRA3, Czech Republic). EDX was carried out on sintered pellets using a Zeiss EVO 40 scanning electron microscope in conjunction with EDX system. To characterize the shape and size of the synthesized MNPs, TEM (PHILIPS, EM) was used at 100 keV. The XRD pattern of Fe_3O_4-chitosan was analyzed (D8 Advance, Bruker, Germany) using graphite monochromatic copper radiation (Cu Kα, λ = 1.54 Å) at 40 kV, 40 mA, and 25 °C. Samples were placed in a zero background metal holder and were scanned from 10° to 80° 2θ with a scanning speed of 2° 2θ min^{-1}. The average diameter, D, of the crystallites of the particles was estimated based on the pure X-ray diffraction broadening, β, using the Scherrer formula[22].

$$D = \frac{K\lambda}{\beta \, Cos \, \theta} \qquad (1)$$

Where, K is the Scherrer's constant of the order of 0.89, approximately equal to the unity and related to the crystallite shape and to the way in which β and D are defined; λ is the X-ray wavelength, β is the full width of half maximum of a diffraction peak, and θ is the diffraction angle.

A VSM (7400, Lakeshare, USA) was applied to determine the magnetic properties of the adsorbent at ±10 kOe at 25 °C. The BET analysis (Quantachrome, 2000, NOVA) was applied to determine the surface area, size, and volume of the pores of the synthesized MNPs and the generated composite. Prior to the measurement, the sample was degassed at 100 ˚A ∘C for 8 h in an out-gassing station to remove any adsorbed water or entrapped gases in the sample.

Fourier transform infrared spectrophotometer (FTIR) spectra of the Fe_3O_4-chitosan composite were obtained using Tensor 27, Bruker, (Germany) model to confirm the functional groups present in it.

2.5. Adsorption study

Batch adsorption studies of fluoride onto magnetic chitosan were conducted in 100-ml Erlenmeyer containing 50 ml of the solution. The effect of variables, such as pH, contact time, different Fe_3O_4-chitosan and fluoride concentrations, and solution temperatures, on the removal efficiency was investigated. To ensure the ideal mixing of the adsorbent and the adsorbate, the Erlenmeyer containing the sample was put on a shaker at 200 rpm for 3 h. After that, the adsorbent was magnetically separated from the solution using a magnet. The remaining fluoride in the solution was determined according to the standard method (4500-D SPADNS method) using the colourimetric method at a wavelength of 570 nm [23]. All of the adsorption tests were carried out in triplicate and the mean and the standard deviation (SD) of the values were used to calculate the final results.

In this study, we initially evaluated the effect of pH on the adsorption capacity in the range of 3-9. Then, the adsorption equilibrium was determined at the optional pH for a time period of 3 h and, subsequently, the adsorption kinetic parameters were calculated. In the next step, we evaluated the effect of fluoride (1-10 mg/L) and the adsorbent (ranging from 0.25-2 g/L) concentrations at the optimal pH and contact time in order to determine the isothermic parameters of the adsorption equilibrium. Finally, we explored the effect of temperature on the adsorption capacity in order to determine the thermodynamic parameters. The removal efficiency as well as the adsorption capacity were calculated using the following equations:

$$\text{Ads.}(\%) = 100 \times (1 - \frac{C_e}{C_o})$$

(2)

$$q_e(mg/g) = \frac{V(C_o - C_e)}{W}$$ (3)

where, q_e is the adsorption capacity (mg/L); C_0 is the initial concentration (mg/L); C_e is the final concentration (mg/l) in the solution; V is the solution volume (L); and W is the mass of the adsorbent (g).

2.6. Desorption and repeated use

The adsorbent reusability and desorption of fluoride loaded on Fe_3O_4-chitosan were performed using five adsorption-regeneration cycles. The performance of fluoride adsorption was investigated with an initial fluoride concentration of 10 mg/L within 180 min under optimal conditions (i.e., a pH of 7 and an adsorbent dose of 1g/L) for five consecutive cycles. At the end of each adsorption cycle, the adsorbent was magnetically separated using a magnet in less than 1 min, and the residual fluoride concentration was determined. After the adsorption, desorption experiments were carried out using 0.1 M HCl, NaOH, and NaCl solutions as desorbent agents. For the desorption studies, samples containing 0.10 g of Fe_3O_4-chitosan loaded with fluoride were shaken at 200 rpm for 24 h with 100 ml of desorbent solutions at 25±1°C. Desorption efficiency was determined as the ratio of the amount of fluoride desorbed to amount of fluoride adsorbed. Afterwards, the regenerated adsorbent was dried in an oven at 100 °C for 60 min and used for the next adsorption-desorption cycle, in order to test the reusability of Fe_3O_4-chitosan for fluoride removal.

3. Results and Discussion

3.1. Characterization of Fe_3O_4-chitosan

Figure 1(a) shows the SEM image of Fe_3O_4-chitosan composite at 15 keV. SEM analysis indicated that the external adsorbent surface has irregular clumps cavities. This rough and course surface could provide more reactive sites and a high adsorption capacity for the synthesized adsorbent. The analysis of EDX (Fig. 1(b)) ensured the presence of elements such as carbon, oxygen, and iron in the synthesized composite structure. The peaks for iron also prove the existence of Fe on the Fe_3O_4-chitosan surface. The analysis also revealed the presence of 16.8 % carbon, 64.9 % oxygen, and 18.3 % iron in the adsorbent structure. Thus, these results suggest that approximately 18% of the surface of chitosan has been occupied by iron in the form of Fe_3O_4 particles. Fig. 1 (c) exhibits the TEM image of Fe_3O_4-chitosan. It can also be clearly seen from the TEM image that Fe_3O_4 particles with an average size of 20-50 nm have a cubic structure and relatively distributed in a uniform way on the surface of chitosan. This confirms that nano-sized Fe_3O_4 particles have been successfully synthesized. Herein, the color of the center of the cubic is darker, verifying the existence of Fe_3O_4.

The specific surface area, volume, and average pore diameter for MNPs and Fe_3O_4-chitosan were measured using the BET method, and the results are given in Table 1. The results indicated that the highest surface area of the MNPs and Fe_3O_4-chitosan were 93.5 and 498.5 m^2/g, respectively, indicating that the composite provides a higher adsorption capacity for pollutants compared to the MNPs. As given in Table 1, the surface area, mean size and volume of pores of Fe_3O_4-chitosan were larger than those of the MNPs, which can be due to the agglomeration of MNPs. The average pore size was estimated to be 2.9 and 3.4 nm for the MNPs and the composite, respectively. According to the IUPAC classification, the average sizes of 2.9 and 3.5 nm can be classified as mesopores groups [24].

According to Fig. 2, the highest magnetization saturation of 46.7, 34.5, and 28.8 emu/g were obtained for Fe_3O_4, Fe_3O_4-chitosan before adsorption, and Fe_3O_4-chitosan after adsorption of fluoride, respectively, which suggests a super-paramagnetic characteristic for the adsorbents.

This rate is much higher than what has been previously reported by researchers as a sufficient magnetization amount [14, 25]. The magnetization value for the Fe_3O_4-chitosan composite was less than that of naked Fe_3O_4, which can be due to the presence of non-magnetic chitosan on the surface of the magnetic particles [17]. As seen in Fig. 2, the observed decrease in the saturation magnetization of the composite was not significant after the adsorption process. This implies that the Fe_3O_4-chitosan composite is a stable adsorbent. These results ensure that the composite can be potentially applied as a magnetic adsorbent to remove contaminants from the aqueous environment to avoid a secondary pollution.

X-ray diffraction (XRD) can provide very useful information about the physical and chemical form of the magnetic particles embedded in the chitosan matrix [17]. The XRD patterns of the samples are shown in Fig. 3 (a). The X-ray pattern of chitosan exhibited characteristic crystalline peaks at $2\theta=8.0^o$ and 20.1^o, respectively. However, these peaks were observed much less intensively in chitosan-carbocycle and Fe_3O_4-chitosan, due to the elimination of the chitosan in the calcination step at 100 ± 2 ^oC [26]. The higher crystallinity of chitosan than its carbocycled compound allowed for better accessibility for fluoride and, thus, higher activity. The synthesized MNPs could take the form of maghemite (Fe_2O_3) or magnetite (Fe_3O_4). Fe_3O_4 is black in color, while Fe_2O_3 has a brown color [27]. After the synthesis process, we observed that the color of the suspension containing the nanoparticles was black, demonstrating the formation of Fe_3O_4 nanoparticles. Fig. 3 (a) indicates the XRD pattern of the synthesized nanoparticles, which is quite similar to that of pure magnetite. Moreover, the absence of peaks correspond to maghemite, ranging from a 2θ angle of $20°$ to $30°$, also verify that the black powder was magnetite. This suggests the lack of impurities in the maghemite. The main peaks at $2\theta =30.1^o$, 35.4^o, 43.1^o, 53.4^o, 56.9^o, and 62.5^o correspond to the (220), (311), (400), (422), (511), and (440) plane of the orthorhombic Fe_3O_4 (JCPDS card no. 19-0629) [13]. The XRD pattern confirmed the presence of Fe_3O_4 particles within the structure of

chitosan, so the prepared composite could be separated from aqueous solutions by magnet. As illustrated in Fig. 4(a), after magnetization of chitosan, the peaks assigned to chitosan ($2\theta=8^{o}$ and 20°) and Fe_3O_4 ($2\theta =30.1^{o}$ and 35.4^{o}) were still observed, indicating successful synthesis of Fe_3O_4 crystals on the chitosan surface. The average particle size of the MNPs was calculated using the Scherrer's equation, which were found to be in the range of 20–51.2 nm. This was in accordance with the results from the TEM analysis.

Since adsorption reactions mostly take place on the surface of the adsorbent, the functional groups on the surface of the adsorbent can play a significant role in the adsorption process. In order to characterize the functional groups on the surface of the samples and to measure the binding mechanism of the pollutants (inorganic or organic), Fourier transform infrared spectroscopy (FTIR) spectra were recorded on a Tensor 27, Bruker, (Germany) spectrometer (Fig. 3(b)). The bonds observed in the range of 3413-3440 cm^{-1} in the spectra of chitosan, chitosan-carbocycle, and Fe_3O_4-chitosan indicated the presence of O-H bond stretching and N-H bond stretching [9, 28, 29]. The bands at 3046 cm^{-1} and 2900 cm^{-1} that can be assigned to the aliphatic stretching vibrations of –CH had very low intensity in the chitosan-carbocycle sample, indicating the presence of residual carbon matter after calcinations [26]. The adsorption at 2927 cm^{-1} and 2860 cm^{-1} is due to the C-H stretching vibration of the -CH_2 groups in chitosan [13]. The bands around 1600 cm^{-1} were assigned to the OH bending vibrational mode due to the adsorption of moisture when FT-IR sample disks were prepared in an open-air atmosphere. According to Figure 3(b), the bonds around 1657 cm^{-1} were observed in the spectra of the chitosan, chitosan-carbocycle, and Fe_3O_4-chitosan samples, which can correspond to C=O of NH=C=O bond stretching. The peak observed at 1366 cm^{-1} can be assigned to C–N stretching vibration. The peaks at 1083 cm^{-1} and 1023 cm^{-1} can be attributed to C-OH bond stretching [17, 30]. For Fe_3O_4 spectra, absorption peaks at 578.6 cm^{-1} can be attributed to Fe-O band vibration of Fe_3O_4. As shown in Fig. 3(b), the FT-IR spectrum of

Fe$_3$O$_4$-chitosan adsorbent was a hybrid of chitosan with Fe$_3$O$_4$ nanoparticles. The spectrum of Fe$_3$O$_4$-chitosan composite peaks at 3430 cm^{-1} due to amine N-H stretching vibration and -OH moieties in the chitosan, at ~1661 cm^{-1} due to N-H scissoring from the primary amine because of free amino groups in the cross-linked chitosan, and at ~580 cm^{-1} for the Fe-O group due to pure Fe$_3$O$_4$ [17]. The FTIR spectrum clearly confirms the existence of chitosan and Fe$_3$O$_4$ in the Fe$_3$O$_4$-chitosan composite.
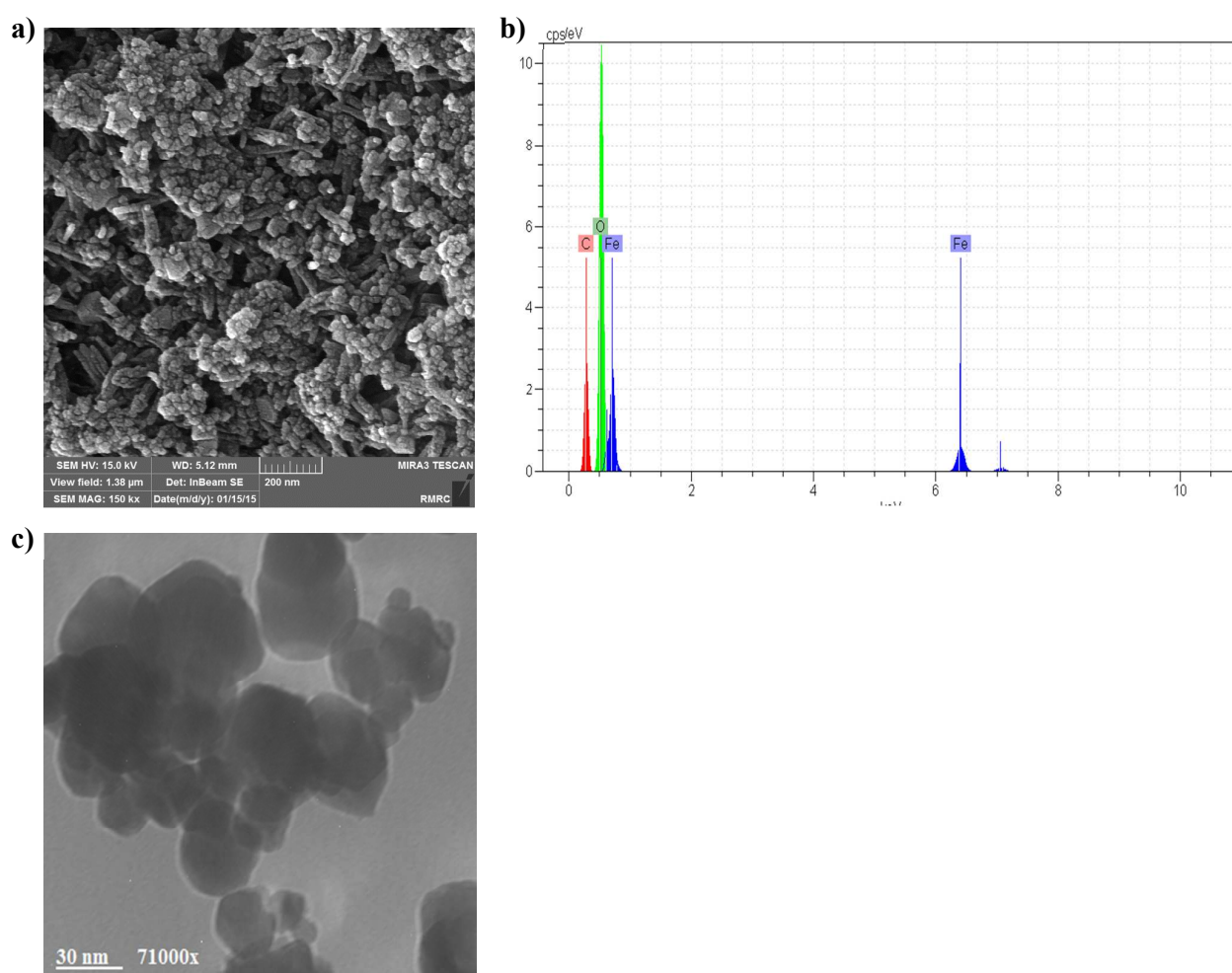

Figure 1. SEM (a) and EDX (b) analysis of Fe$_3$O$_4$-chitosan composite and TEM image (c) for MNPs.

Table 1

Textural characteristics of Fe$_3$O$_4$-chitosan composite.

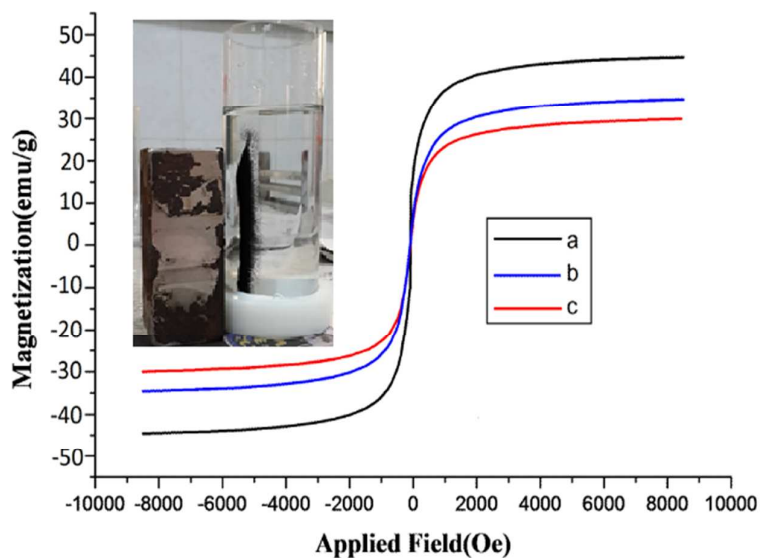| Adsorbent	Surface area (m^2/g)	Pore volume (cm^3/g)	Mean pore diameter (nm)	Pores structure
MNPs	93.5	2.37	2.9	Mesopore
Fe$_3$O$_4$-chitosan	498.5	3.68	3.4	Mesopore

Figure 2. (a) Magnetization curve of (a) Fe$_3$O$_4$, (b) Fe$_3$O$_4$-chitosan before adsorption and (c) Fe$_3$O$_4$-chitosan after adsorption of fluoride and magnetically separation of the Fe$_3$O$_4$-chitosan from solution (insert).
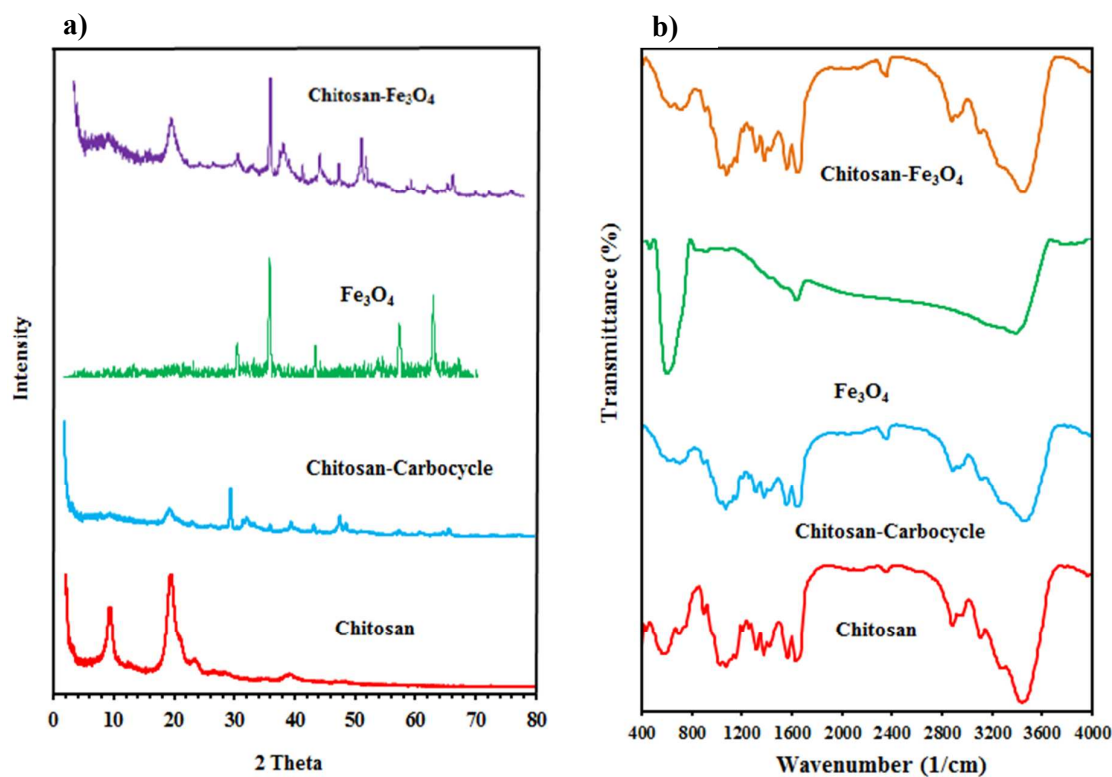
Figure 3. (a) XRD pattern and (b) FTIR spectra of chitosan, chitosan-carbocycle, Fe_3O_4, and Fe_3O_4-chitosan composite.

3.2. Adsorption process optimization

3.2.1. Effect of initial solution pH

It has been reported that the efficiency of fluoride adsorption is highly dependent on the initial pH of the solution. Similar results were also observed in our work, which are illustrated in Fig. 4. It illustrates the impact of solution pH on the fluoride removal efficiency by Fe_3O_4-chitosan. As can be seen, the removal efficiency increased with an increase in the pH from 3 to 7, while slightly decreasing afterwards (up to a pH of 9). The maximum removal efficiency (85%) was observed at pH 7. These findings are in good agreement with those of previous studies for several sorbent-fluoride sorption processes [2, 31]. Since the concentration of OH^- ions is higher at alkaline pHs, the competition between OH^- and fluoride ions on the active sites of Fe_3O_4-chitosan led to a decrease in the adsorption efficiency [32].

Hence, the pH 7 was selected as the optimal pH for the rest of the experiments, which is in accordance with the optimal pH for the adsorption of fluoride on other adsorbents [2, 33, 34]. However, it is noteworthy that the variations in the removal efficiency were not significant under acidic and basic conditions; the removal efficiency was 78.8 and 81% for pH 3 and 9, respectively. This demonstrates that the Fe_3O_4-chitosan still provides very good fluoride uptake in media with various pHs. Therefore, it can be concluded that the Fe_3O_4-chitosan is capable of satisfactorily removing fluoride from aqueous solutions even without pH adjustment. In addition, the pH of fluoride-contaminated groundwater usually ranges between 6 and 8. Therefore, the adsorption by Fe_3O_4-chitosan could become a sound alternative in full-scale fluoride removal facilities as the pH range is wide.
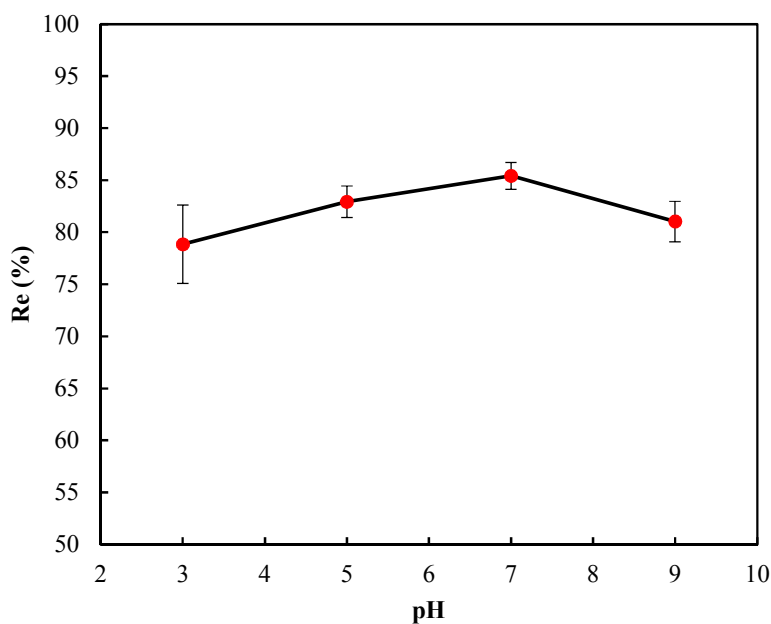

Figure 4. Impact of the pH on the fluoride removal efficiency by Fe_3O_4-chitosan composite (conditions: Adsorbent dose= 0.5 g/L, Contact time= 60 min, initial fluoride concentration= 5 mg/L and temperature= 20±1°C).

3.2.2. Adsorption kinetics

15

The effect of contact time on the removal efficiency of fluoride by Fe_3O_4-chitosan was evaluated in a time period of 3 h, the results of which are indicated in Fig. 5. This experiment was carried out at an initial fluoride concentration of 5 mg/L, a pH 7 (optimum), and an adsorbent dose of 0.5 g/L. As shown in the Fig. 5, the removal process was very quick in the first 60 min of the experiment, while no significant removal was observed afterwards, implying that the adsorption process reaches the equilibrium in 60 min. The rapid increase of the adsorption capacity in the initial stages may be due to the existence of enormous vacant active sites in the adsorbent surface. Then, as the time passes, these active sites are filled by the adsorbate, which finally leads to a saturated adsorbent surface [35]. Generally, increasing of contact time decreases the availability of the adsorbate ions to unoccupied active sites on the adsorbent surface, and these sites ultimately become saturated when the process reaches the equilibrium state [35]. Therefore, we selected this contact time (60 min) as the equilibrium time for the next experiments. This equilibrium time (60 min) was also observed in previous studies of fluoride adsorption on other adsorbents such as carbon [34], chitosan supported mixed metal oxides beads[2], and $Fe_3O_4@Al(OH)_3$ [36].

In the present work, we employed four kinetic models, including pseudo-first-order, pseudo-second-order, intraparticle diffusion, and Elovich models, to investigate the kinetics of fluoride adsorption onto the Fe_3O_4-chitosan. The equations for each of the models are as follows:

Pseudo-first-order: $Ln(q_e-q_t)=lnq_e-k_ft$ (4)

pseudo-second-order: $t/q_t=t/q_e+1/k_s \, q_e^2$ (5)

Elovich: $q_t= \beta \, ln(\alpha\beta)+ \beta \, lnt$ (6)

Intraparticle diffusion: $q_t=k_i \, t^{0.5}$ (7)

where, q_t and q_e (mg/g) are the adsorption capacity of the adsorbent at equilibrium and at time t; K_1 (L/min) and K_2 (mg/g.min) are the coefficients of reaction rate for the pseudo-first-order and the pseudo-second-order models; α(mg/g.min) and β (g/mg) are the initial adsorption rate and the activation energy for chemical adsorption; K_i (mg/g.min 0.5) is the constant rate for the intraparticle diffusion model; and C_i (mg/g) is the constant indicating the boundary layer effects.

Table 2 presents the values of kinetic models parameters for fluoride adsorption onto Fe_3O_4-chitosan. Results of the kinetic models showed that the adsorption kinetics of fluoride can be better described by the pseudo-second-order model. According to the r^2 values, the pseudo-second-order model had the best fit with the experimental data, implying that the concentrations of both the adsorbent and the adsorbate were the rate-controlling step for the process of fluoride adsorption onto the Fe_3O_4-chitsan [15]. This also suggests that chemisorption was the dominant mechanism in the adsorption process, which involves the exchange or sharing of electrons between fluoride and the binding sites on the magnetic chitosan particles [37]. It has been reported that the chemisorption process that is limited to one layer of molecules on the surface of the adsorbent is commonly followed by added layers of the physically adsorbed molecules of the adsorbate [38].

The pseudo-second-order of the adsorption process was also strongly confirmed by the very good agreement between the calculated q_e and the experimental q_e values. This finding was also confirmed by the curves presented in Fig. 5. Our results are in-line with those of the previous works [9, 33, 34], in which the authors reported that the pseudo-second-order model had the best fit with their experimental data.

We also applied the intraparticle diffusion model to investigate the possibility of pore diffusion, in which the ions of the adsorbate transport from the solution to the pores in the adsorbent due mainly to the stirring applied to the batch process [15]. However, the low r^2 value

(0.66) of the intraparticle diffusion model implied that the pore diffusion is not the rate controlling step. This is also consistent with the findings of the study of Ma et al [33]. As observed in Table 2, the value of C_i was measured to be 3.08 mg/g, indicating that intraparticle diffusion is not the only controlling step for fluoride adsorption and the process is also controlled, to some extent, by boundary layer diffusion [15, 39].

Table 2
Adsorption kinetic models constants of fluoride adsorption onto Fe_3O_4-chitosan

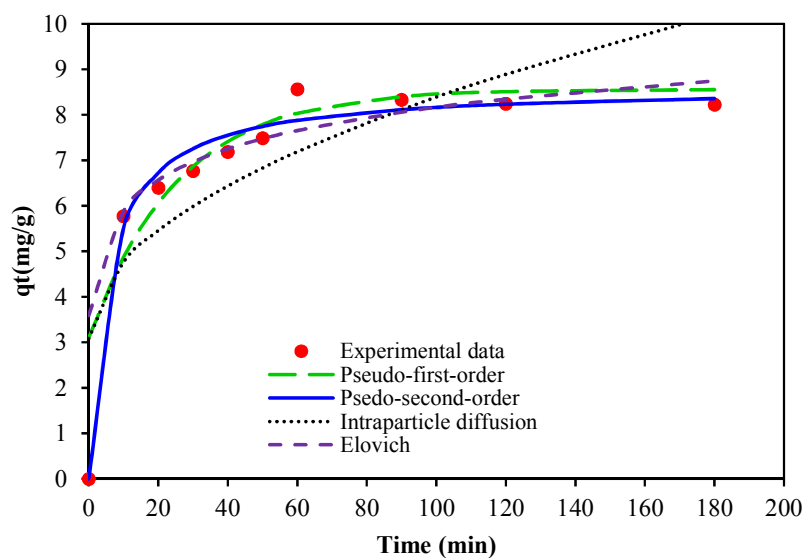| Kinetic models	Parameters	Values
Pseudo-first-order		
	$q_{e, Cal}(mg/g)$	5.45
	$k_1(min^{-1})$	0.039
	r^2	0.877
Pseudo-second-order		
	$q_{e,Cal}(mg/g)$	8.62
	$k_2(g/mg)(min^{-1})$	0.02
	r^2	0.997
Elovich		
	α	37.38
	β	0.993
	r^2	0.936
Intraparticle diffusion		
	k_i	0.53
	C_i	3.08
	r^2	0.665
Experimental q_e		**8.36**

Figure 5. Effect of contact time (3 h) on the removal efficiency of fluoride by Fe_3O_4-chitosan composite (conditions: Adsorbent dose= 0.5 g/L, initial fluoride concentration= 5 mg/L and temperature= 20±1°C).

3.2.3. Effect of adsorbent dose

Fig. 6 illustrates the variations of the removal efficiency (%, left axis) and adsorption capacity (mg/g, right axis) at different adsorbent doses (0.25-2 g/L), a pH of 7, a contact time of 60 min, and an initial fluoride concentration of 5 mg/L. As can be seen from the figure, the removal efficiency increased significantly by an increase in the adsorbent dose, from approximately 60% at the adsorbent dose of 0.25 g/L to about 92% at a dose of 2 g/L. On the other hand, the adsorption capacity had a dramatic decrease with increasing adsorbent doses; the adsorption capacity decreased from 12 mg/g down to approximately 2.3 mg/g when the adsorbent dose increased from 0.25 g/L to 2 g/L. This can be justified by the fact that increased adsorbent dose increases the accessibility of active sites on the pores of the Fe_3O_4-chitosan to the fluoride ions, which leads to an enhanced removal efficiency [15, 35]. However, increased adsorbent dose most likely increases particle interactions, such as aggregation, which results from a high sorbent concentration; this leads to a significant reduction in the active surface area of the adsorbent and, consequently, reduces its adsorption capacity [40, 41]. This can also be explained by the decrease in the ratio of fluoride per mass unit of adsorbent. Similar effect has been reported for the adsorbent dose by previous studies[42].
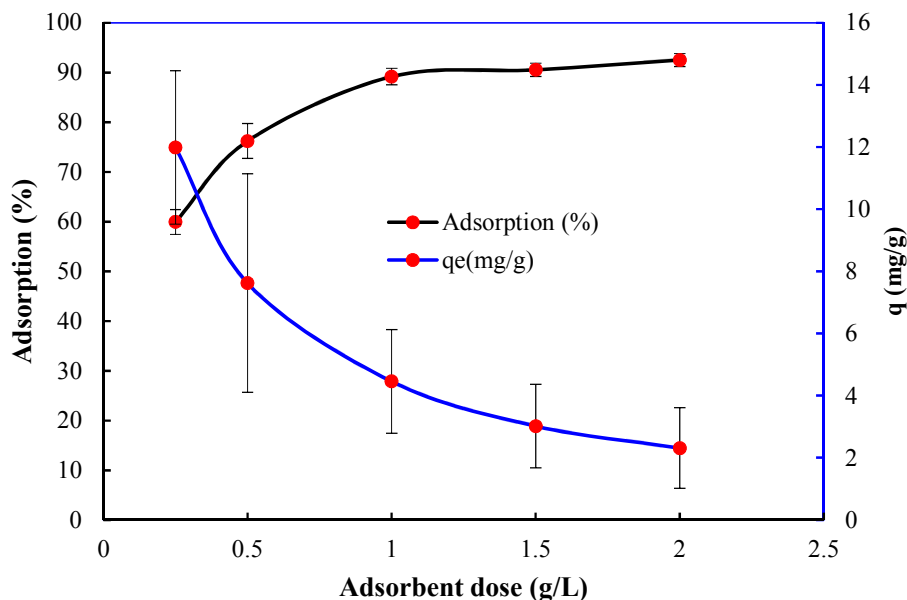
Figure 6. Effect of adsorbent dose on the removal efficiency and the adsorption capacity of Fe$_3$O$_4$-chitosan composite (conditions: pH=7, Contact time= 60 min, initial fluoride concentration= 5 mg/L and temperature= 20±1°C).

3.2.4. Adsorption isotherms

Analysis of the equilibrium data is important in designing adsorption systems. In the present work, we applied three isotherm models, namely Langmuir, Freundlich, and Temkin, to investigate the behavior of fluoride adsorption onto Fe$_3$O$_4$-chitsan. The following equations were used for the isotherm models:

Langmuir: $C_e/q_e=C_e/q_0+1/k_Lq_0$ (8)

Freundlich: $lnq_e=lnk_F+n^{-1} lnC_e$ (9)

Temkin: $q_e=B ln K_T+B ln C_e$ (10)

where, k_L is an empirical constant related to the adsorption energy; k_f and $1/n$ are constants reflecting the adsorption capacity and intensity [43]; B= RT/bT, and bT is a constant related to the adsorption heat (J/mol), T is temperature; R is the universal gas constant (8.314 J/mol K);

20

k_t (L/mg) is the binding constant at equilibrium which indicates the maximum amount of binding energy [14].

The results of the fluoride adsorption isotherm modeling experiments, which were conducted at a pH of 7, an adsorbent dose of 1 g/L, a contact time of 60 min, and operational temperatures of 20, 35, and 50 ºC are presented in Table 3. As presented in the table, the values of correlation coefficients (r^2) were larger than 0.95 for Langmuir and Freundlich isotherm models, indicating that both models fit very well with the experimental data. Similar findings have been reported in the literature for the removal of fluoride by different types of adsorbents [29, 36]. However, the Freundlich isotherm model had the best fit with the experimental data; r² values of above 0.99 for all studied temperatures. This implies that the process of fluoride adsorption onto Fe_3O_4-chitosan follows a heterogeneous (multi-layer) mechanism. This finding was also confirmed by the good agreement between the equilibrium data for the fluoride adsorption experiments and the Freundlich equilibrium isotherm, as shown in Fig. 7. The desirability of the adsorption process was confirmed by the Freundlich exponent, *n*, since its value was $1 < n < 10$ at all temperatures [15, 36]. Based on the Langmuir model, the maximum adsorption capacities improved with increasing of solution temperatures, indicating the occurrence of an endothermic process.

The k_f and n values reported in Table 3 for the Freundlich isotherm model, which respectively represent adsorption capacity and intensity, were found to increase by increasing of operational temperature; the k_f and n values increased from 5.97 and 2.16 at 20 ºC to 7.05 and 2.6 at 50 ºC, respectively. This indicates that the adsorption capacity and intensity increased with increasing of operational temperature, which is an indicator of the chemisorption mechanism for the adsorption of fluoride onto Fe_3O_4-chitosan and further substantiates our previous results presented earlier [44, 45].
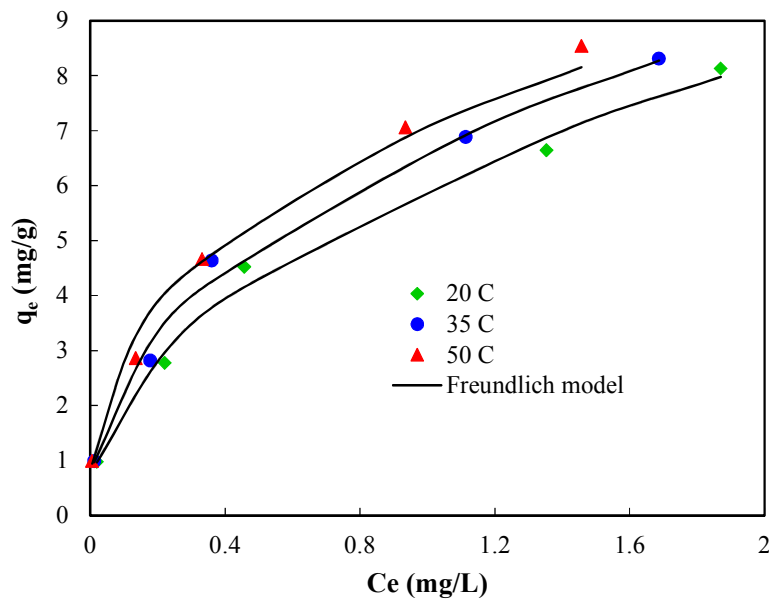
Figure 7. Freundlich isotherm model and experimental data of fluoride adsorption on Fe_3O_4-chitosan composite (conditions: pH=7, Adsorbent dose= 1 g/L, Contact time= 60 min, initial fluoride concentration= 1-10 mg/L and temperature= 20-35°C).

Table 3

The isothermic parameters calculated at equilibrium based on each model for the process of fluoride adsorption onto magnetic chitosan particles.

Isotherm models		Constants	
Langmuir	k_L	$q_m(mg/g)$	r^2
20°C	2.57	9.26	0.956
35°C	3.45	9.34	0.964
50°C	4.41	9.43	0.958
Freundlich	K_f	n	r^2
20°C	5.971	2.16	0.996
35°C	6.606	2.32	0.993
50°C	7.056	2.6	0.992
Temkin	k_t	B	r^2
20°C	61.29	1.505	0.906
35°C	101.92	1.429	0.9
50°C	217.76	1.278	0.869

The maximum adsorption capacity, q_m, of the Fe_3O_4-chitosan was compared with the fluoride adsorption capacities of other adsorbents (Table 4). Based on the Langmuir equilibrium

model, the maximum level of fluoride uptake per unit mass of Fe_3O_4-chitosan was 9.43 mg/g.

It is noticeable from Table 4 that the Fe_3O_4-chitosan has a higher maximum adsorption

capacity compared to other adsorbents. The observed differences in the adsorption capacities

for the listed adsorbents can be due to structure, surface area, and the properties of functional

groups in each adsorbent.

Table 4
Comparison of adsorption capacity of MB between various adsorbents found in the
literatures.

Adsorbent	pH	Temp. (°C)	Isotherm	Kinetic	q_m (mg/g)	References
Hydrous ferric oxide doped alginate beads	7.0	29	Freundlich	Pseudo-second order	8.9	[46]
Meso porous Al-chitosan	7.0	30±3	Langmuir	Pseudo-second order	8.26	[26]
Chitosan supported mixed oxide beads	7.0	50	Langmuir	Not done	6.48	[2]
Activated alumina	7.0	-	Langmuir	Pseudo-first-order	2.41	[47]
Fe(III) carboxylated chitosan	7.0	50	Freundlich	intraparticle diffusion	12.34	[48]
Hydrous ferric oxide	6.5	24±1	Langmuir	Pseudo-second order	6.71	[29]
Pine bark biochar	2.0	25 35 45	Langmuir	****	9.77 10.53 8.4	[49]
Cerium loaded silica gel/chitosan (Ce-SGCS)	7.0	50	Langmuir	Pseudo-second order	10.54	[9]
Magnetic Corn stover biochar (MCSBC)	2.0	25	-	pseudo-first order	4.11	[50]
Chitosan supported zirconium(IV) tungstophosphate composite	7.0	50	Freundlich	pseudo-second-order and intraparticle diffusion	9.901	[51]
Alumina/chitosan composite	7.0	50	Freundlich	Pseudo-second order	23.81	[28]
Polypyrrole/Fe_3O_4 magnetic nanocomposite	6.5	45	Langmuir–Freundlich	Pseudo-second order	17.6-22.3	[52]
Fe_3O_4-chitsan	7.0	50	Freundlich	Pseudo-second order	9.43	The present work

3.2.5. Adsorption Thermodynamics

In the present work, we also investigated the thermodynamics of fluoride adsorption onto

Fe_3O_4-chitsan, aiming to provide a deeper understanding of the process. For this purpose, the

removal efficiency was calculated at three different temperatures, i.e. 20, 35, and 50 ºC, and

the thermodynamic parameters were also determined using the following equations [44]:

$$\ln(K_o) = -\frac{\Delta H^o}{RT} + \frac{\Delta S^o}{R} \Rightarrow K_o = \frac{q_e}{C_e}$$

$$\qquad\qquad\qquad\qquad\qquad\qquad\qquad (11)$$

$$\Delta G^o = -RT \ln K_o \qquad\qquad\qquad (12)$$

where, ΔS^o is the amount of energy change (J/mol K); ΔG^o is the Gibbs free energy (Kj/mol);

ΔH^o is the change in the enthalpy (Kj/mol); K_o is the distribution coefficient; C_e is the

equilibrium concentration of the adsorbate in the solution (mg/L); q_e is the amount of fluoride

adsorbed at the equilibrium (mg/g). Table 5 presents the calculated thermodynamic

parameters for the conducted experiments.

Table 5

The calculated thermodynamic parameters of the adsorption fluoride on the Fe_3O_4-chitsan.

Temperature (K)	ΔG^o(kJ/mol)	ΔH^o(kJ/mol)	ΔS^o(kJ/mol.K)
293	-5.5	10.36	0.54
308	-6.54		
323	-7.1		

As given in the table, the value of ΔS^o was positive, indicating that Fe_3O_4-chitosan particles

have affinity for fluoride ions. The negative values of ΔG^o suggest that the adsorption process

was feasible and had a spontaneous nature [53]. Furthermore, it can be observed that the

absolute values of $-\Delta G^o$ increased with increasing of operational temperature; the absolute $-$

ΔG^o value rose from $-$ 5.5 KJ/mol at 20 ºC to -7.1 at 50 ºC. This indicates that the adsorption

of fluoride ions onto Fe_3O_4-chitosan is more favorable at higher temperatures [15]. Moreover,

studies have suggested that the observed increase in the absolute value of ΔG^o at higher

24

operational temperatures is most likely because both the adsorbent and the adsorbate dry out; this, in turn, facilitates the chemical reaction between the two and leads to more favorable conditions for the adsorption process at higher operational temperatures. The positive value obtained for $\Delta H°$ shows that fluoride adsorption onto Fe_3O_4-chitosan is an endothermic reaction [15]. Similar results ($+\Delta S°$, $-\Delta G°$ and $+\Delta H°$) have been obtained for the adsorption of fluoride ions on other adsorbents such as Fe(III) loaded carboxylated chitosan beads [48], chitosan supported mixed metal oxides beads [2], and alumina/chitosan composite [28].

3.3. Reusability and stability of Fe_3O_4-chitosan

The regeneration and reuse of adsorbents are likely to be a key factor in evaluating their potential for commercial applications. The results of five adsorption–regeneration cycles are shown in Fig. 8 (a and b). The removal efficiency of fluoride by Fe_3O_4-chitosan decreased from 64.8% to 61.4% after five cycles. This confirms that the Fe_3O_4-chitosan can be reused for at least 5 successive cycles while maintaining high adsorption efficiency. Hence, it can be concluded that the Fe_3O_4-chitosan can be applied in the treatment of contaminated waters as a reusable adsorbent.

Results from the desorption study indicated that for all cycles, the desorption ability of HCl is higher than those of other desorbing solutions. According to Fig. 8(b), HCl solution could desorb 93.6% of fluoride from Fe_3O_4-chitosan surface in the first cycle. It was also observed that the desorption efficiency did not noticeably change in the next desorption cycles; the desorption efficiency of fluoride by HCl decreased from 93.6 to 88.5% after five cycles. This high desorption efficiency may be explained by the protonation of the adsorbent surface with an acidic agent [54]. This observation showed that the Fe_3O_4-chitosan can be easily recovered with acid treatment. Hence, it can be used as an economical and effective adsorbent for fluoride removal from water due to its high potential for reusability. The stability of the

adsorbent was evaluated through determining the concentrations of the dissolved iron ions in the solution during the five consecutive cycles. It was observed that the concentrations of the dissolved iron ions in the solution were at a minimal level (<0.2 mg/L) during all the cycles; this was below the maximum acceptable iron concentration in drinking water, i.e. 0.3 mg/L, set by the WHO [1]. This ensures that leaching of iron from Fe_3O_4-chitosan surface might not cause metal pollution in water. Therefore, it can be concluded that Fe_3O_4-chitosan exhibited good stability and can be applied as a promising adsorbent to remove fluoride from contaminated water with negligible loss of its magnetic properties.
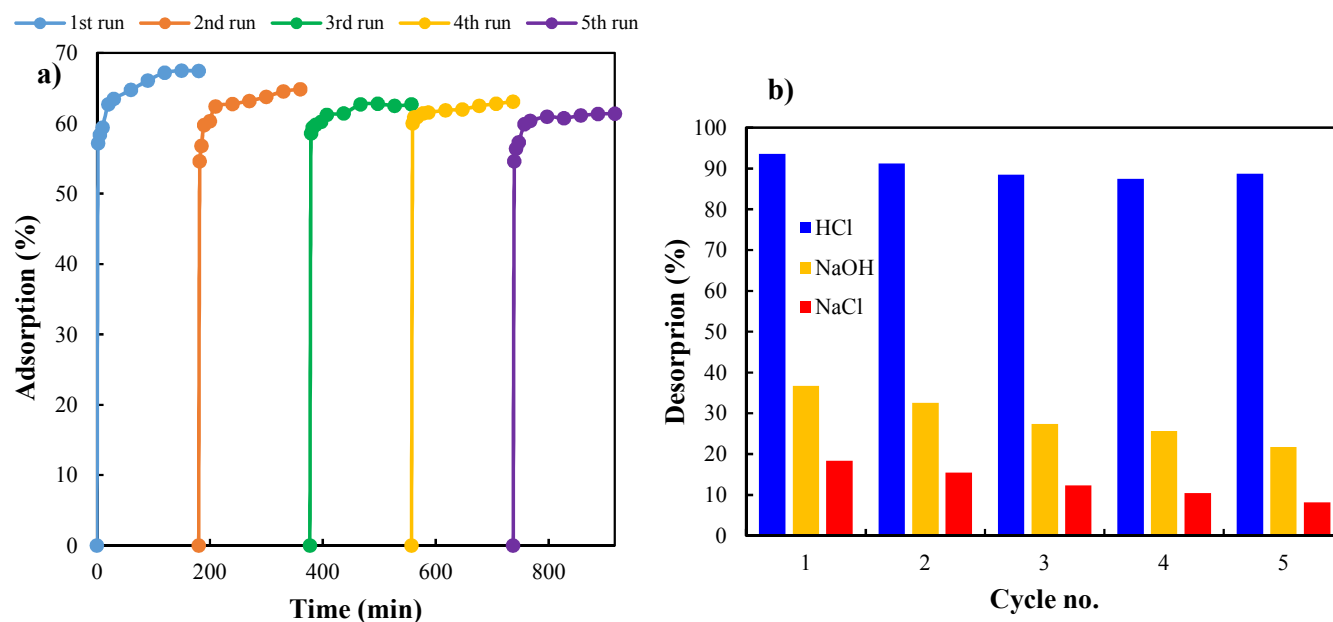

Figure 8. (a) Recycling results for the adsorption of fluoride by Fe_3O_4-chitosan composite in aqueous solutions and desorption and (b) fluoride desorption from Fe_3O_4-chitosanusing several desorbing solutions for five cycle.

4. Conclusion

Chitosan is a copolymer with favorable biological characteristics; due to its excellent adsorption properties, it has been widely used, alone or in combination with other materials,

for the removal of a variety of environmental contaminants. In the present study, chitosan was used in combination of Fe_3O_4 magnetite nanoparticles (MNPs) for the preparation of a magnetic composite (Fe_3O_4-chitosan), which was used as an adsorbent for the removal of fluoride from water. Our results indicated that at a pH of 7 ± 0.2, the adsorption efficiency increased by an increase in the temperature, contact time, and adsorbent dosage, and a decrease in the initial fluoride concentration. Thermodynamic studies indicated that the adsorption process was feasible, spontaneous, and endothermic. Desorption experiments suggested that the Fe_3O_4-chitosan can be easily reused for at least five successive cycles while maintaining high adsorption efficiency. It can be concluded that the magnetization of adsorbents and use of magnetic separation techniques can be an effective way to resolve problems associated with separation and filtration.

Acknowledgment

Conflict of interest

The authors have declared no conflict of interest.

Author Contributions

Conceived and designed the experiments: AMB RRK BK. Performed the experiments: AA AK. Analyzed the data: RRK BK AA. Contributed reagents/materials/analysis tools: AMB BK AK. Wrote the paper: RRK BK.

References

1.   W. H. Organization, *Guidelines for drinking-water quality: First addendum to volume 1, Recommendations*, World Health Organization, 2006.
2.   S. M. Prabhu and S. Meenakshi, *J. Water Process Eng.*, 2014, 2, 96-104.

3. A. K. Yadav, C. Kaushik, A. K. Haritash, A. Kansal and N. Rani, *J. Hazard. Mater.*, 2006, 128, 289-293.
4. S. Venkata Mohan, S. Ramanaiah, B. Rajkumar and P. Sarma, *Bioresource Technol.*, 2007, 98, 1006-1011.
5. X. Fan, D. Parker and M. Smith, *Water Res.*, 2003, 37, 4929-4937.
6. Y. Ku and H.-M. Chiou, *Water, air, Soil Pollu.*, 2002, 133, 349-361.
7. J. Zhu, H. Zhao and J. Ni, *Sep. Purif. Technol.*, 2007, 56, 184-191.
8. K. Hu and J. M. Dickson, *J. Membrane Sci.*, 2006, 279, 529-538.
9. S. M. Prabhu and S. Meenakshi, *J. Water Process Eng.*, 2014, 3, 144-150.
10. R. Jayakumar, M. Prabaharan, R. Reis and J. Mano, *Carbohyd. Polym.*, 2005, 62, 142-158.
11. M. H. Farzana and S. Meenakshi, *J. Chitin Chitosan Sci.*, 2013, 1, 50-58.
12. N. Viswanathan and S. Meenakshi, *J. App. Polym. Sci.*, 2009, 112, 1114-1121.
13. Y. Du, M. Pei, Y. He, F. Yu, W. Guo and L. Wang, *Plos One*, 2014, 9, e108647.
14. S. Nethaji, A. Sivasamy and A. Mandal, *Bioresource Technol.*, 2013, 134, 94-100.
15. B. Kakavandi, A. Esrafili, A. Mohseni-Bandpi, A. J. Jafari and R. R. Kalantary, *Water Sci. Technol.*, 2014, 69, 147-155.
16. Y. Haldorai, D. Kharismadewi, D. Tuma and J.-J. Shim, *Korean J. Chem. Eng.*, 2015, 1-6.
17. D. H. K. Reddy and S.-M. Lee, *Adv. Colloid Interface Sci.*, 2013, 201, 68-93.
18. N. N. Thinh, P. T. B. Hanh, T. V. Hoang, V. D. Hoang, L. H. Dang, N. Van Khoi and T. Dai Lam, *Mater. Sci. Eng.: C*, 2013, 33, 1214-1218.
19. C. Dong, W. Chen and C. Liu, *App. Surf. Sci.*, 2014, 292, 1067-1076.
20. Y. Xu and W.-x. Zhang, *Ind. Eng. Chem. Res.*, 2000, 39, 2238-2244.
21. M. Fan, P. Yuan, T. Chen, H. He, A. Yuan, K. Chen, J. Zhu and D. Liu, *Chinese Sci. Bull.*, 2010, 55, 1092-1099.
22. A. D. Eaton, L. S. Clesceri and A. E. Greenberg, *Washington, DC*, 2005, 20001-23710.
23. L. Huang, Y. Sun, W. Wang, Q. Yue and T. Yang, *Chem. Eng. J.*, 2011, 171, 1446-1453.
24. T. Depci, *Chem. Eng. J.*, 2012, 181, 467-478.
25. D. H. K. Reddy and S.-M. Lee, *Adv. Colloid Iinterface Sci.*, 2013, 201, 68-93.
26. S. Jagtap, M. Yenkie, N. Labhsetwar and S. Rayalu, *Micropor. Mesopor. Mater.*, 2011, 142, 454-463.
27. S. Shariati, M. Faraji, Y. Yamini and A. A. Rajabi, *Desalination*, 2011, 270, 160-165.
28. N. Viswanathan and S. Meenakshi, *J. Hazard. Mater.*, 2010, 178, 226-232.
29. T. Nur, P. Loganathan, T. Nguyen, S. Vigneswaran, G. Singh and J. Kandasamy, *Chem. Eng. J.*, 2014, 247, 93-102.
30. G. Huang, H. Zhang, J. X. Shi and T. A. Langrish, *Ind. Eng. Chem. Res.*, 2009, 48, 2646-2651.
31. C. N. Rao and J. Karthikeyan, *Water Air Soil Pollut.*, 2012, 223, 1101-1114.
32. Q. Zhou, X. Lin, B. Li and X. Luo, *Chem. Eng. J.*, 2014, 256, 306-315.
33. W. Ma, F.-Q. Ya, M. Han and R. Wang, *J. Hazard. Mater.*, 2007, 143, 296-302.
34. Y. Yu, C. Wang, X. Guo and J. P. Chen, *J. Colloid Interface Sci.*, 2015, 441, 113-120.
35. B. Kakavandi, A. Jonidi Jafari, R. Rezaei Kalantary, S. Nasseri, A. Ameri and A. Esrafily, *J. Environ. Health Sci. Eng.*, 2013, 10, 1-9.
36. X. Zhao, J. Wang, F. Wu, T. Wang, Y. Cai, Y. Shi and G. Jiang, *J. Hazard. Mater.*, 2010, 173, 102-109.
37. M. D. G. de Luna, E. D. Flores, D. A. D. Genuino, C. M. Futalan and M.-W. Wan, *J.Taiw. Inst. Chem. Eng.*, 2013, 44, 646-653.

38. M. Momčilović, M. Purenović, A. Bojić, A. Zarubica and M. Ranđelović, *Desalination*, 2011, 276, 53-59.
39. B. Kakavandi, R. Rezaei Kalantary, M. Farzadkia, A. H. Mahvi, A. Esrafili, A. Azari, A. R. Yari and A. B. Javid, *J. Environ. Health. Sci. Eng.*, 2014, 12, 1-10.
40. M. M. Rao, D. Ramana, K. Seshaiah, M. Wang and S. Chien, *J. Hazard. Mater.*, 2009, 166, 1006-1013.
41. A. Azari, B. Kakavandi, R. R. Kalantary, E. Ahmadi, M. Gholami, Z. Torkshavand and M. Azizi, *J. Porous Mater.*, 2015, 22, 1083-1096.
42. K. Li, Y. Zhang, Y. Dang, H. Wei and Q. Wang, *CLEAN–Soil Air Water*, 2014, 42, 1549-1557.
43. H. Lalhruaitluanga, K. Jayaram, M. Prasad and K. Kumar, *J. Hazard. Mater.*, 2010, 175, 311-318.
44. B. Kakavandi, R. Rezaei Kalantary, A. Jonidi Jafari, S. Nasseri, A. Ameri, A. Esrafili and A. Azari, *Clean-Soil, Air, Water*, 2014, Accepted Manuscript.
45. S. K. Nadavala, K. Swayampakula, V. M. Boddu and K. Abburi, *J. Hazard. Mater.*, 2009, 162, 482-489.
46. M. Sujana, A. Mishra and B. Acharya, *App. Surf. Sci.*, 2013, 270, 767-776.
47. S. Ghorai and K. Pant, *Sep. Purif. Technol.*, 2005, 42, 265-271.
48. N. Viswanathan and S. Meenakshi, *J. Fluorine Chem.*, 2008, 129, 503-509.
49. D. Mohan, R. Sharma, V. K. Singh, P. Steele and C. U. Pittman Jr, *Ind. Eng. Chem. Res.*, 2012, 51, 900-914.
50. D. Mohan, S. Kumar and A. Srivastava, *Ecol. Eng.*, 2014, 73, 798-808.
51. N. Viswanathan, C. Sairam Sundaram and S. Meenakshi, *J. Hazard. Mater.*, 2009, 167, 325-331.
52. M. Bhaumik, T. Y. Leswifi, A. Maity, V. V. Srinivasu and M. S. Onyango, *J. Hazard. Mater.*, 2011, 186, 150-159.
53. S. Zhou, Y. Shao, N. Gao, J. Deng and C. Tan, *CLEAN–Soil Air Water*, 2013, 41, 539-547.
54. R. Rezaei Kalantry, A. Jonidi Jafari, A. Esrafili, B. Kakavandi, A. Gholizadeh and A. Azari, *Desalination and Water Treatment*, 2015, 1-12.